

Spinless mirror Chern insulator from projective symmetry algebra

Lubing Shao,^{1,2} Zhiyi Chen,¹ Kai Wang¹, Shengyuan A. Yang³, and Yuxin Zhao^{4,*}

¹National Laboratory of Solid State Microstructures and Department of Physics, Nanjing University, Nanjing 210093, China

²Collaborative Innovation Center of Advanced Microstructures, Nanjing University, Nanjing 210093, China

³Research Laboratory for Quantum Materials, Singapore University of Technology and Design, Singapore 487372, Singapore

⁴Department of Physics and HK Institute of Quantum Science & Technology, The University of Hong Kong, Pokfulam Road, Hong Kong, China



(Received 23 September 2021; revised 16 October 2023; accepted 24 October 2023; published 13 November 2023)

It was commonly believed that a mirror Chern insulator (MCI) must require spin-orbital coupling, since time-reversal symmetry for spinless systems contradicts with the mirror Chern number. So MCI cannot be realized in spinless systems, which include the large field of topological artificial crystals. Here, we disprove this common belief. The first point to clarify is that the fundamental constraint is not from spin-orbital coupling but the symmetry algebra of time-reversal and mirror operations. Then, our theory is based on the conceptual transformation that the symmetry algebras will be *projectively* modified under gauge fields. Particularly, we show that the symmetry algebra of mirror reflection and time reversal required for MCI can be achieved projectively in spinless systems with lattice \mathbb{Z}_2 gauge fields, i.e., by allowing real hopping amplitudes to take \pm signs. Moreover, we propose the basic structure, the twisted π -flux blocks, to fulfill the projective symmetry algebra, and develop a general approach to construct spinless MCIs based on these building blocks. Two concrete spinless MCI models are presented, which can be readily realized in artificial systems such as acoustic crystals.

DOI: [10.1103/PhysRevB.108.205126](https://doi.org/10.1103/PhysRevB.108.205126)

I. INTRODUCTION

The field of topological matter started with the discovery of the quantum Hall effect or the Chern insulator (CI) [1–3]. A Chern insulator requires the breaking of time-reversal (\mathcal{T}) symmetry, which poses difficulty for its realization. For example, a strong magnetic field is needed for the quantum Hall effect [1]; and for the renowned Haldane model [3], its delicate flux configuration is not easy to achieve in practical systems [4]. Later, a significant breakthrough is the discovery of symmetry-protected topological insulators without breaking \mathcal{T} . The prominent ones include the \mathcal{T} -invariant topological insulator [5,6] and the mirror Chern insulator (MCI) [7–9]. The \mathcal{T} -invariant topological insulator has found realization in many materials, which led to the boom of the entire field in the past fifteen years [10–13]. Meanwhile, MCI initiated the field of crystalline topological states, which is still actively explored today [14–17].

There is a common wisdom regarding MCI: With \mathcal{T} invariance, MCI must require spin-orbit coupling (SOC) [7,18,19]. Hence, MCI can only be realized in spinful systems, but not spinless systems. In other words, \mathcal{T} -invariant spinless MCI does not exist. Because of this, while MCI has been realized in electronic systems of several materials [8,9,19], it was believed to be forbidden for artificial systems, such as acoustic/photonic crystals, electric-circuit arrays, and mechanical network systems, as these systems are intrinsically spinless. Qualitatively different from the symmetry-protected

topological many-body wavefunctions, the artificial crystals can effectively simulate the topological band structures of one Bloch particle by their high tunability. However, despite the rapid growth of topological artificial crystals into a huge and active field in recent years [20–30], MCI has never been achieved in such systems so far.

In this paper, we overturn this common wisdom. We show that spinless MCI does exist, and it can be readily realized in artificial systems such as acoustic crystals. This discovery is made possible by advances in two aspects. First, we scrutinize the fundamental requirement for a MCI and clarify that the key factor is not SOC but the symmetry algebra. Explicitly, the only necessary condition is that the mirror operator \mathcal{M} must satisfy $\mathcal{M}^2 = -1$ for MCI, provided that it commutes with \mathcal{T} . Second, for spatial symmetries such as \mathcal{M} , the algebra can be controlled by implementing lattice gauge field. Particularly, we show that spinless MCI can be achieved by the simple \mathbb{Z}_2 gauge field, meaning that the hopping amplitudes are allowed to take \pm signs, which is something that can be readily engineered in artificial crystals [25,31–36]. Under gauge fields, symmetries would satisfy so-called projective algebra, which can be designed to meet the requirement of MCI. The notion of projective symmetry algebra was applied to physics initially in the study of quantum spin liquids [37]. Its profound implications for topological states were only revealed very recently [38–44], and some predictions have already been successfully verified in experiments with acoustic crystals [35,36,45,46]. Here, we find that distinct from the previous cases, MCIs need an essentially different mechanism and lattice design. We propose a general prescription to construct MCIs based on a twisted π -flux block. We show that for any

*yuxinphy@hku.hk

CI model, we can generate an associated spinless MCI using the twisted blocks. We explicitly demonstrate our method via two famous CI models, namely the triangular-lattice model and the Hofstadter model. Our proposed MCI designs can be easily realized in artificial crystals.

II. SYMMETRY ALGEBRAS OF MCI

Let us start by analyzing the symmetry algebra required for MCI. There are 2D and 3D MCIs. For a 2D MCI, the mirror symmetry is with respect to the 2D plane of the system. For a 3D MCI, the mirror Chern number is defined on a 2D subsystem, i.e., some mirror-invariant plane, in the Brillouin zone. Hence, without loss of generality, we focus on 2D MCIs for clarity.

We find that the fundamental symmetry condition for a MCI is the following algebra [47]:

$$[\mathcal{T}, \mathcal{M}] = 0, \quad \mathcal{M}^2 = -1. \quad (1)$$

To understand this, we first note that with the \mathcal{M} symmetry, states of the system can be separated into the mirror-even and mirror-odd subspaces. Particularly, the momentum-space Hamiltonian $\mathcal{H}(\mathbf{k})$ can be put into the block diagonal form

$$\mathcal{H}(\mathbf{k}) = \begin{bmatrix} h_+(\mathbf{k}) & 0 \\ 0 & h_-(\mathbf{k}) \end{bmatrix}, \quad (2)$$

in accord with the two eigenspaces of \mathcal{M} . If the algebra (1) holds, \mathcal{M} has eigenvalues of $\pm i$. For eigenstates $|\psi_{\pm}\rangle$ with $\mathcal{M}|\psi_{\pm}\rangle = \pm i|\psi_{\pm}\rangle$, we observe that $\mathcal{M}\mathcal{T}|\psi_{\pm}\rangle = \mathcal{T}\mathcal{M}|\psi_{\pm}\rangle = \mathcal{T}(\pm i|\psi_{\pm}\rangle) = \mp i\mathcal{T}|\psi_{\pm}\rangle$, since \mathcal{T} is an anti-unitary operator involving complex conjugation. This just means that \mathcal{T} exchanges the two eigenspaces. Hence, we must have $uh_+^*(-\mathbf{k})u^\dagger = h_-(\mathbf{k})$ for some unitary matrix u determined by \mathcal{T} , i.e., \mathcal{T} transforms $h_{\pm}(\mathbf{k})$ into $h_{\mp}(\mathbf{k})$. Assuming that $\mathcal{H}(\mathbf{k})$ is gapped, we can calculate Chern numbers C_{\pm} for $h_{\pm}(\mathbf{k})$, respectively. Since \mathcal{T} inverses the Chern number, $h_+(\mathbf{k})$ and $h_-(\mathbf{k})$ must have opposite Chern numbers, $C_+ = -C_-$. Thus, although the total Chern number $C = C_+ + C_- = 0$, each block h_{\pm} can have a nontrivial Chern number, and accordingly C_+ is defined as the mirror Chern number [7].

From the above reasoning, we see that the essence for a nontrivial mirror Chern number is: \mathcal{T} must *exchange* the eigenspaces of \mathcal{M} . For electronic systems with SOC, $\mathcal{T} = i\sigma_2\hat{K}\hat{I}$ and $\mathcal{M} = i\sigma_3$ in the spin space of each electron, where σ 's are the Pauli matrices. Hence, the algebra in (1) is naturally satisfied. In comparison, if $\mathcal{M}^2 = +1$ and $[\mathcal{T}, \mathcal{M}] = 0$, as for typical spinless systems, then \mathcal{T} would preserve the eigenspaces of \mathcal{M} . This is because the eigenvalues ± 1 of \mathcal{M} are real numbers that commutes with \mathcal{T} . Although we still can write $\mathcal{H}(\mathbf{k})$ into the block diagonal form (2) for eigenspaces of ± 1 , both $h_{\pm}(\mathbf{k})$ are invariant under \mathcal{T} , and therefore they each must have a zero Chern number, i.e., $C_{\pm} = 0$.

We have some remarks before proceeding. First, contrary to common perceptions, the relation $\mathcal{T}^2 = \pm 1$ is not essential for MCI, since \mathcal{T} inverses the Chern number in both cases. Second, it is clear from the analysis that the key factor here is not SOC but the symmetry algebra, particularly, whether \mathcal{M}^2 equals $+1$ or -1 .

III. PROJECTIVE SYMMETRY ALGEBRA

Although it seems from experience that spinless systems always have $\mathcal{M}^2 = +1$, we show that with certain \mathbb{Z}_2 gauge fields the condition in (1) can be realized as projective symmetry algebra in spinless systems.

Let us start with some general considerations on a mirror symmetric system with a given \mathbb{Z}_2 gauge configuration. The field is described by a chosen configuration of gauge connections, i.e., signs ± 1 of real hopping amplitudes. The gauge-connection configuration in general is not invariant under the spatial mirror reflection M , but will be changed to another equivalent configuration (another gauge choice), which is related to the original one by a \mathbb{Z}_2 gauge transformation \mathbf{G} . \mathbf{G} is specified by assigning a sign of $+1$ or -1 to the basis at each site. Then, the physical mirror operator will be represented as the combination

$$\mathcal{M} = \mathbf{G}M, \quad (3)$$

namely the spatial reflection M followed by the gauge transformation \mathbf{G} . Since both M and \mathbf{G} in real space are real matrices, $[\mathcal{M}, \mathcal{T}] = 0$ in (1) is trivially satisfied. Moreover, since $M^2 = \mathbf{G}^2 = 1$, to satisfy $\mathcal{M}^2 = -1$ in (1), we need the anticommutation relation between \mathbf{G} and M ,

$$\{\mathbf{G}, M\} = 0. \quad (4)$$

The anticommutativity is equivalent to $M\mathbf{G}M^{-1} = -\mathbf{G}$, which just means that M inverses all signs at all sites for \mathbf{G} . This observation is a guiding principle for the model construction.

Let us consider a simple system consisting of only four sites, as illustrated in Fig. 1. Positive and negative hopping amplitudes are marked with blue and red colors, respectively. For the model in Fig. 1(a), the Hamiltonian is given by

$$\mathcal{H} = J_R\tau_0 \otimes \sigma_1 + J_I\tau_2 \otimes \sigma_2, \quad (5)$$

where τ 's and σ 's be two sets of Pauli matrices, which respectively operate on the row and column indices of the block. The mirror reflection $M = \tau_1 \otimes \sigma_0$ through the dashed horizontal line exchanges diagonal and antidiagonal hopping processes, and therefore the gauge connections are changed. To restore the original gauge connections, the gauge transformation $\mathbf{G} = \tau_3 \otimes \sigma_0$ needed is specified in the middle of Fig. 1(a). Obviously, M inverses \mathbf{G} with $\{M, \mathbf{G}\} = 0$. Hence, Eq. (4) is satisfied, and the resulting projective symmetry algebra will be (1) needed for the MCI, where

$$\mathcal{M} = \mathbf{G}M = i\tau_2 \otimes \sigma_0. \quad (6)$$

On the other hand, the setup, $\mathcal{H}^{(b)} = J_1\tau_1 \otimes \sigma_0 + J_2\tau_3 \otimes \sigma_1$, in Fig. 1(b) does not work. In the middle of Fig. 1(b), the gauge transformation $\mathbf{G}' = \tau_0 \otimes \sigma_3$ is invariant under M , and therefore $[\mathbf{G}', M] = 0$ rather than $\{\mathbf{G}', M\} = 0$, and we have $\mathcal{M}'^2 = +1$ with $\mathcal{M}' = \tau_1 \otimes \sigma_3$ in this case.

The arrangement in Fig. 1(a) is referred to as a twisted π -flux block, because, as shown in Fig. 1(c), it is a twist of a π -flux rectangle with $\mathcal{H}^{(c)} = -J_1\tau_1 \otimes \sigma_3 + J_2\tau_0 \otimes \sigma_1$. It is clear that both the π flux and the twist are essential for achieving the symmetry algebra (1). In fact, there are eight possible \mathbb{Z}_2 gauge-connection configurations on this twisted π -flux block [see Figs. 2(b) and 2(c)], which are equivalent

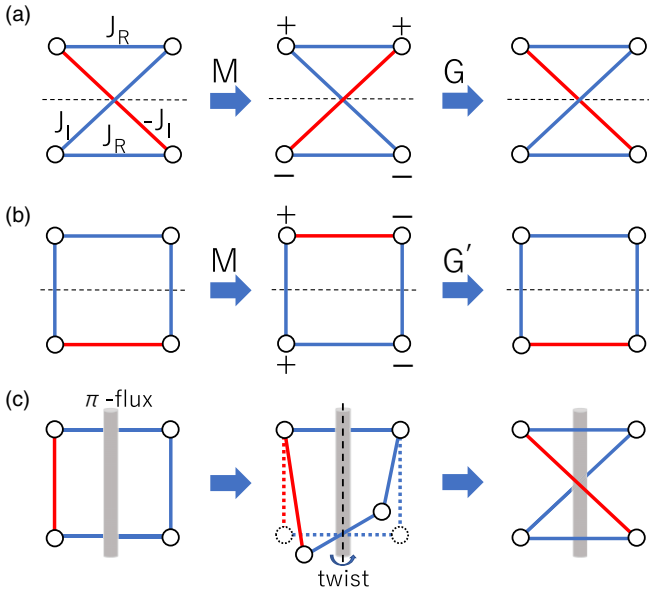


FIG. 1. Two four-site tight-binding models. Red and blue lines denote negative and positive hopping amplitudes, respectively. The dashed horizontal lines in (a) and (b) are the reference lines for the spatial mirror reflection M . The signs on the middle figures specify the gauge transformations G and G' for (a) and (b), respectively. The tight-binding models are invariant under M followed by G or G' . (c) The model in (a) is a twist of a rectangle with flux π . The π flux is depicted by a thin gray tube.

to each other through some \mathbb{Z}_2 gauge transformations, and therefore all can realize the projective algebra (1).

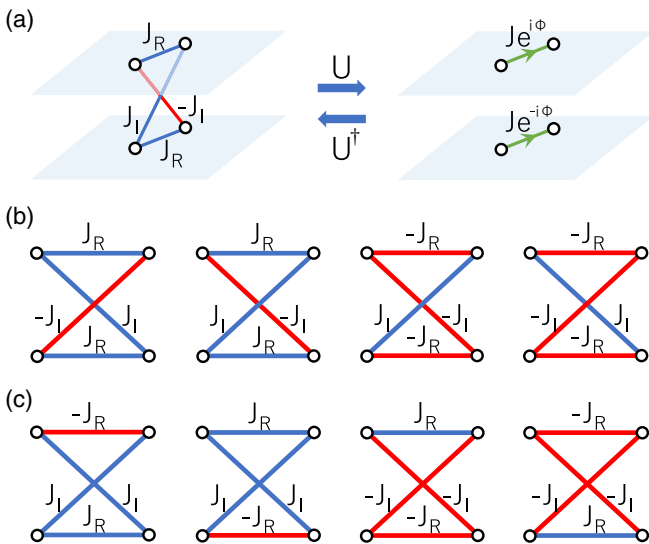


FIG. 2. (a) The equivalence mapping between the twisted π -flux block and two complex hopping amplitudes. U is the unitary transformation diagonalizing \mathcal{M} . (b) Four twisted π -flux blocks with $\mathcal{M} = i\tau_2 \otimes \sigma_0$. (c) The other four with $\mathcal{M} = i\tau_2 \otimes \sigma_3$.

IV. GENERAL METHOD FOR CONSTRUCTING SPINLESS MCI

We develop a general method for constructing spinless MCIs. Our construction is based on the twisted π -flux block. Since the blocks in Figs. 2(b) and 2(c) are gauge equivalent, it is sufficient to look into one of them. Consider the one in Fig. 1(a) with the Hamiltonian (5) and mirror operator (6).

It is enlightening to view the model in the eigenspaces of \mathcal{M} , which can be achieved by performing the unitary transformation $U = \exp(-i\tau_1 \otimes \sigma_0 \pi/4)$. Under the transformation, $\mathcal{M} \rightarrow U\mathcal{M}U^\dagger = i\tau_3 \otimes \sigma_0$. Now, τ_3 corresponds to the index of the two eigenspaces of \mathcal{M} with eigenvalues $\pm i$, and the Hamiltonian is transformed into the block diagonal form

$$U\mathcal{H}U^\dagger = \begin{bmatrix} J_R\sigma_1 + J_I\sigma_2 & 0 \\ 0 & J_R\sigma_1 - J_I\sigma_2 \end{bmatrix}_\tau. \quad (7)$$

Meanwhile, \mathcal{T} is transformed to be $U\mathcal{T}U^\dagger = -i\tau_1\hat{\mathcal{K}}$, which, as expected, exchanges the two diagonal blocks of the Hamiltonian, i.e., the two eigenspaces of \mathcal{M} . We refer to the two diagonal blocks as eigenvalue layers. Then, $J_R\sigma_1 \pm J_I\sigma_2$ can be interpreted as hopping amplitudes $Je^{\pm i\phi}$ between two lattice sites in each eigenvalue layer, as illustrated in Fig. 2(a). The hopping phase and strength are explicitly given by

$$e^{i\phi} = (J_R + iJ_I)/J, \quad J = \sqrt{J_R^2 + J_I^2}. \quad (8)$$

It is important that starting from a spinless model with purely real hopping amplitudes, we are able to convert it to a system with complex hopping amplitudes. Conversely, for any prescribed complex hopping amplitude, we can construct a spinless twisted π -flux block such that one of its eigenvalue layer realizes the amplitude. Note that the hopping phase is a key ingredient for CI models. For instance, the Haldane model is characterized by the second-neighbor hopping phase ϕ on a honeycomb lattice [3,48,49]. For the Hofstadter model, each square plaquette has a flux ϕ [50,51].

Based on this understanding, we have the following general method to construct spinless MCIs from any CI model. Given such a CI model $H_C(\phi)$ with a characteristic phase $e^{i\phi}$, we can construct a spinless MCI $H_{MC}(\phi)$ protected by \mathcal{M} and \mathcal{T} by the invertible mapping illustrated in Fig. 2(a). Specifically, we take $H_C(\phi)$ and $H_C(-\phi)$ as two independent layers. Then, we perform the mapping in Fig. 2(a) inversely, i.e., replace each pair of complex hopping amplitudes with phases $\pm\phi$ on the two layers by a twisted π -flux block. The resultant bilayer tight-binding model is just the wanted spinless MCI. For this system, the mirror operator is $\mathcal{M} = i\tau_2$ with τ 's operating on the layer degrees of freedom, and $\mathcal{T} = \hat{\mathcal{K}}$.

The corresponding mapping for the momentum-space Hamiltonians can be immediately constructed. Let $h_C(\mathbf{k}, \phi)$ be the momentum-space Hamiltonian for $H_C(\phi)$. Then, we introduce

$$h_\pm(\mathbf{k}, \phi) = \frac{1}{2}[h_C(\mathbf{k}, \phi) \pm h_C(\mathbf{k}, -\phi)]. \quad (9)$$

$h_+(\mathbf{k}, \phi)$ [$h_-(\mathbf{k}, \phi)$] is an even (odd) function of ϕ . Since $h_C(\mathbf{k}, \phi)$ and $h_C(\mathbf{k}, -\phi)$ are related by \mathcal{T} symmetry, $h_+(\mathbf{k}, \phi)$ [$h_-(\mathbf{k}, \phi)$] are also even (odd) under \mathcal{T} operation. Then, the \mathcal{T} -invariant Hamiltonian $\mathcal{H}_{MC}(\mathbf{k}, \phi)$ for the bilayer MCI is

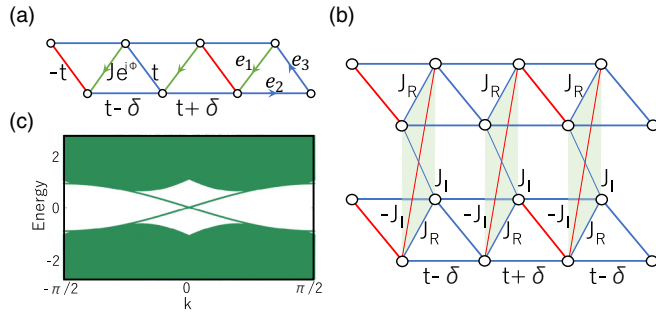


FIG. 3. (a) The triangular-lattice CI model. Green, red, and blue bonds denote complex, negative, and positive hopping amplitudes, respectively. The model is dimerized by δ along e_2 . (b) The corresponding MCI model. Complex hopping amplitudes in (a) are replaced by twisted π -flux blocks. (c) The spectrum of the bilayer model with edges along e_2 . The parameter values are chosen as $t = 1$, $\delta = 0.5$, $J_R = J \cos \phi$, $J_I = J \sin \phi$ with $J = 2$ and $\phi = 2\pi/5$ [52].

given by

$$\mathcal{H}_{MC}(\mathbf{k}) = \begin{bmatrix} h_+(\mathbf{k}, \phi) & -ih_-(\mathbf{k}, \phi) \\ ih_-(\mathbf{k}, \phi) & h_+(\mathbf{k}, \phi) \end{bmatrix}_{\tau}. \quad (10)$$

Finally, we should substitute ϕ by J_R and J_I according to Eq. (8). Here, $\mathcal{M} = i\tau_2$, and $\mathcal{T} = \hat{\mathcal{K}}\hat{I}$ with \hat{I} the inversion of momenta.

In the above discussion, we have chosen the particular twisted π -flux block in Fig. 1(a) to demonstrate our idea. Other blocks in Figs. 2(b) and 2(c) can also be used. It is not difficult to see that these eight blocks can be put into two groups, with members in a group sharing the same representation of \mathcal{M} : For those in Fig. 2(b), $\mathcal{M} = i\tau_2 \otimes \sigma_0$; whereas for Fig. 2(c), $\mathcal{M} = i\tau_2 \otimes \sigma_3$, the detail of which is given in Appendix A. It should be noted that if one uses more than one kind of blocks in a single model, then these blocks should be chosen from only one of the two groups to maintain the same representation for \mathcal{M} .

Nevertheless, we emphasize that generically chiral edge states of the two mirror layers in Fig. 2(a) will be simultaneously excited in real space, since mirror reflection relates two real-space layers.

V. CONCRETE MODELS

We demonstrate our theory by constructing two concrete spinless MCIs from well-know CI models.

The first one is based on the triangular-lattice CI model illustrated in Fig. 3(a). Let us denote the three bond vectors as e_a with $a = 1, 2, 3$. The hopping amplitudes along e_1 are $Je^{i\phi}$, and the phase $e^{i\phi}$ characterizes the model. The other hopping amplitudes are real, and those along the e_3 bonds change signs alternatively in the e_2 direction. The hopping amplitudes along e_3 is t , and the hoppings along e_2 have a dimerized pattern with amplitudes $t \pm \delta$. If $J > t$ and $\delta \neq 0$, the model can realize a CI by tuning ϕ , and the Chern number $C = \pm 1$ as can be seen in Appendix B. The corresponding spinless MCI model is illustrated in Fig. 3(b). Following our general method, it is a bilayer model with each original bond with phase ϕ replaced by a twisted π -flux block, and the Hamiltonian is in the form

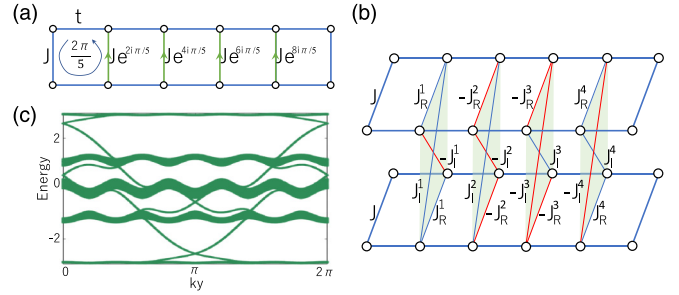


FIG. 4. (a) The Hofstadter model. The flux ϕ is $2\pi/5$. Green, red, and blue bonds denote complex, negative, and positive hopping amplitudes, respectively. (b) The corresponding Hofstadter MCI model. The green bonds are replaced by the four twisted π -flux blocks in Fig. 2(b). (c) The spectrum of the MCI model with edges along the y direction. The parameter values are chosen as $t = J = 1$, and accordingly $J_R^n = J |\cos 2n\pi/5|$ and $J_I^n = J |\sin 2n\pi/5|$ with $n = 1, 2, 3, 4$ [52].

of (10), which is given in Appendix B. The spectrum with the open boundary conditions for an edge along e_2 is shown in Fig. 3(c). We see a pair of left-handed and right-handed topological edge bands, which correspond to the unit mirror Chern number.

The second example is based on the renowned Hofstadter CI model [50,51]. It is just a square-lattice model with flux ϕ per square plaquette. Here, we choose $\phi = 2\pi/5$. The unit cells for the Hofstadter model and the corresponding MCI model are illustrated in Figs. 4(a) and 4(b). We choose to connect the two layers of the MCI by using the four different twisted π -flux blocks in Fig. 2(b), so that the required flux in each eigenspace layer of \mathcal{M} can be realized. The model has four energy gaps separating energy bands into five groups. Ordered by energy, the mirror Chern numbers for these five groups of bands are found as $-1, -1, 4, -1$, and -1 , which is given in Appendix C. The topological chiral edge bands emerge accordingly, as shown in Fig. 1(c). Particularly, for the middle two gaps, each hosts two left-handed and two right-handed chiral bands, since the sums of mirror Chern numbers below them are ± 2 , respectively.

VI. DISCUSSION

We have disproved the common belief that MCI must require SOC and hence can only be realized in spinful systems. Essentially, we have clarified the most fundamental symmetry requirement for MCIs and how \mathbb{Z}_2 gauge fields can projectively modify the symmetry algebra to achieve the requirement in spinless systems. Although we have focused on 2D spinless MCIs, the discussion can be directly extended to 3D spinless MCI models.

Our paper greatly broadens the experimental relevance of MCIs. Our proposed spinless MCI models can be readily realized in acoustic crystals with engineerable \mathbb{Z}_2 gauge fields [32–36,36,45]. Particularly, an acoustic realization of the twisted π -flux blocks is given in detail in Appendix D. Other artificial crystals, such as cold atoms in optical lattices [53,54] and electric-circuit arrays [26,27], may also be possible platforms for realizing our proposals.

ACKNOWLEDGMENTS

This work is supported by National Natural Science Foundation of China (Grants No. 12275126, No. 12174181, and No. 12161160315) and Basic Research Program of Jiangsu Province (Grant No. BK20211506).

APPENDIX A: TWISTED π -FLUX BLOCK

The twisted π -flux block is essential for the construction of mirror Chern insulators in the main text. Under the unitary transformation U diagonalizing the projective representation of mirror symmetry \mathcal{M} , the Hamiltonian of twisted π flux can be transformed into block diagonal form. Here we provide the detailed analysis of the Hamiltonian for the twisted π -flux block as shown in Fig. 2 of the main text.

The four twisted π -flux blocks in Fig. 2(b) are invariant under $\mathcal{M}_1 = \mathbf{G}_1 M$, where

$$\mathbf{G}_1 = \tau_3 \otimes \sigma_0, \quad M = \tau_1 \otimes \sigma_0. \quad (\text{A1})$$

Obviously, they satisfy the anticommutation relation $\{\mathbf{G}_1, M\} = 0$, and $\mathcal{M}_1 = i\tau_2 \otimes \sigma_0$. The operation of the mirror symmetry \mathcal{M}_1 in this case is illustrated by Fig. 1(a) in the main text. By the unitary transformation $U = e^{-i\pi\tau_1 \otimes \sigma_0/4}$ as given in the main text, \mathcal{M}_1 can be diagonalized as $U\mathcal{M}_1U^\dagger = i\tau_3 \otimes \sigma_0$. For the block in Fig. 2(a), its Hamiltonian can be written as

$$\mathcal{H} = J_R\tau_0 \otimes \sigma_1 + J_I\tau_2 \otimes \sigma_2, \quad (\text{A2})$$

where J_R and J_I are positive. By the unitary transformation U , the Hamiltonian can be transformed as

$$U\mathcal{H}U^\dagger = \begin{bmatrix} J_R\sigma_1 + J_I\sigma_2 & \\ & J_R\sigma_1 - J_I\sigma_2 \end{bmatrix}. \quad (\text{A3})$$

Hence, the Hamiltonian $U\mathcal{H}U^\dagger$ contains two blocks, which is represented in the right panel of Fig. 2(a). By the same transformation, we collect the detailed mapping of the four building blocks in Fig. 2(b) in the following as

$$\mathcal{H}_1 = J_R\tau_0 \otimes \sigma_1 - J_I\tau_2 \otimes \sigma_2$$

$$U\mathcal{H}_1U^\dagger = (J_R\sigma_1 - J_I\sigma_2) \oplus (J_R\sigma_1 + J_I\sigma_2), \quad (\text{A4})$$

$$\mathcal{H}_2 = J_R\tau_0 \otimes \sigma_1 + J_I\tau_2 \otimes \sigma_2$$

$$U\mathcal{H}_2U^\dagger = (J_R\sigma_1 + J_I\sigma_2) \oplus (J_R\sigma_1 - J_I\sigma_2), \quad (\text{A5})$$

$$\mathcal{H}_3 = -J_R\tau_0 \otimes \sigma_1 + J_I\tau_2 \otimes \sigma_2$$

$$U\mathcal{H}_3U^\dagger = (-J_R\sigma_1 + J_I\sigma_2) \oplus (-J_R\sigma_1 - J_I\sigma_2), \quad (\text{A6})$$

$$\mathcal{H}_4 = -J_R\tau_0 \otimes \sigma_1 - J_I\tau_2 \otimes \sigma_2$$

$$U\mathcal{H}_4U^\dagger = (-J_R\sigma_1 - J_I\sigma_2) \oplus (-J_R\sigma_1 + J_I\sigma_2). \quad (\text{A7})$$

The four transformed Hamiltonians contain two blocks, and the first blocks represent the systems of two sites with the hopping coefficients as $Je^{-i\phi}$, $Je^{i\phi}$, $Je^{i(\pi-\phi)}$, and $Je^{i(\pi+\phi)}$, respectively. Here, we have taken $J_R = J \cos \phi$ and $J_I = J \sin \phi$.

The four twisted π -flux blocks in Fig. 2(c) are invariant under $\mathcal{M}_2 = \mathbf{G}_2 M$ with

$$\mathbf{G}_2 = \tau_3 \otimes \sigma_3, \quad M = \tau_1 \otimes \sigma_0, \quad (\text{A8})$$

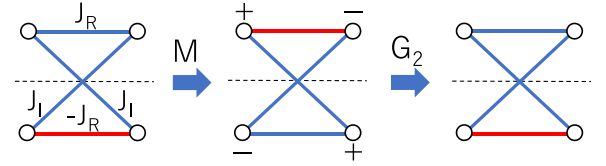


FIG. 5. The operation of $\mathcal{M}_2 = \mathbf{G}_2 M$.

by which we have

$$\mathcal{M}_2 = i\tau_2 \otimes \sigma_3, \quad (\text{A9})$$

and the algebra $[\mathcal{T}, \mathcal{M}_2] = 0$, $\mathcal{M}_2^2 = -1$ of Eq. (1) in the main text is also satisfied. The operation of mirror symmetry \mathcal{M}_2 is illustrated in Fig. 5, which is the second building block of Fig. 2(c). Here, time-reversal symmetry is represented as $\mathcal{T} = \mathcal{K}$ with \mathcal{K} the complex conjugation. The Hamiltonian can be written as

$$\mathcal{H} = J_R\tau_3 \otimes \sigma_1 + J_I\tau_1 \otimes \sigma_1. \quad (\text{A10})$$

Obviously, it satisfies $[\mathcal{M}_2, \mathcal{H}] = 0$. By the unitary transformation $U = e^{-i\pi\tau_1 \otimes \sigma_3/4}$, \mathcal{M}_2 can be diagonalized as $U\mathcal{M}_2U^\dagger = i\tau_3 \otimes \sigma_0$. Similarly, the Hamiltonian is transformed into diagonal blocks as

$$U\mathcal{H}U^\dagger = (J_R\sigma_1 + J_I\sigma_2) \oplus (-J_R\sigma_1 + J_I\sigma_2). \quad (\text{A11})$$

Note that time-reversal symmetry is now represented in the eigenspace of \mathcal{M} as

$$\mathcal{T} = \tau_1 \otimes \sigma_3 \mathcal{K}. \quad (\text{A12})$$

Then, for the four twisted π -flux blocks in Fig. 2(c), the Hamiltonians are transformed as

$$\mathcal{H}_5 = -J_R\tau_3 \otimes \sigma_1 + J_I\tau_1 \otimes \sigma_1$$

$$U\mathcal{H}_5U^\dagger = (-J_R\sigma_1 + J_I\sigma_2) \oplus (J_R\sigma_1 + J_I\sigma_2), \quad (\text{A13})$$

$$\mathcal{H}_6 = J_R\tau_3 \otimes \sigma_1 + J_I\tau_1 \otimes \sigma_1$$

$$U\mathcal{H}_6U^\dagger = (J_R\sigma_1 + J_I\sigma_2) \oplus (-J_R\sigma_1 + J_I\sigma_2), \quad (\text{A14})$$

$$\mathcal{H}_7 = J_R\tau_3 \otimes \sigma_1 - J_I\tau_1 \otimes \sigma_1$$

$$U\mathcal{H}_7U^\dagger = (J_R\sigma_1 - J_I\sigma_2) \oplus (-J_R\sigma_1 - J_I\sigma_2), \quad (\text{A15})$$

$$\mathcal{H}_8 = -J_R\tau_3 \otimes \sigma_1 - J_I\tau_1 \otimes \sigma_1$$

$$U\mathcal{H}_8U^\dagger = (-J_R\sigma_1 - J_I\sigma_2) \oplus (J_R\sigma_1 - J_I\sigma_2). \quad (\text{A16})$$

The first blocks of the Hamiltonians $U\mathcal{H}_{5,6,7,8}U^\dagger$ are the systems of two sites with the hopping coefficients as $Je^{i(\pi-\phi)}$, $Je^{i\phi}$, $Je^{-i\phi}$, and $Je^{i(\pi+\phi)}$, respectively.

APPENDIX B: TRIANGLE-LATTICE MODEL

We give the detail of triangle-lattice model in the main text here. The monolayer triangle-lattice model is illustrated in Fig. 3(a). The three edges of each triangle are $\mathbf{e}_{1,2,3}$. The hopping coefficient along each \mathbf{e}_1 is $Je^{i\phi}$. There is the dimerization along \mathbf{e}_2 with hopping amplitudes as $t - \delta$ and $t + \delta$. Each unit cell consists of two sites, and the unit vectors can now be chosen as $2\mathbf{e}_2$, \mathbf{e}_3 . The hopping amplitude along \mathbf{e}_3 is $\pm t$, where in Fig. 3(a) the signs \pm are marked by blue and red

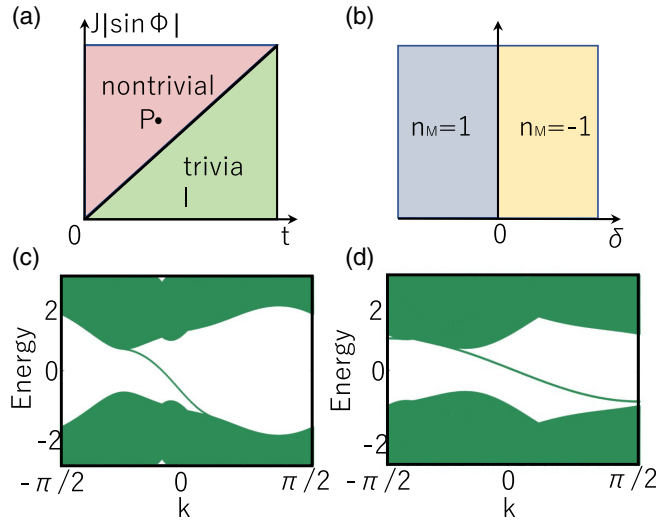


FIG. 6. (a) The phase diagram of monolayer system when $\delta \neq 0$. (b) The phase diagram of monolayer system when $t < J|\sin \phi|$. (c) and (d) are the energy spectra for the monolayer model with open boundary conditions along \mathbf{e}_1 and \mathbf{e}_2 , respectively. The parameters in calculating (c) and (d) are set as $t = 1$, $\delta = 0.5$, $\phi = 2\pi/5$, and $J = 2$.

lines, respectively. Hence, the Hamiltonian of the monolayer triangular lattice is given as

$$h_C(\mathbf{k}, \phi) = [2J \cos(\mathbf{k} \cdot \mathbf{e}_1 - \phi) + 2t \cos \mathbf{k} \cdot \mathbf{e}_2] \sigma_1 + 2\delta \sin \mathbf{k} \cdot \mathbf{e}_2 \sigma_2 - 2t \cos \mathbf{k} \cdot \mathbf{e}_3 \sigma_3. \quad (\text{B1})$$

The gap of energy spectrum is closed if

$$t = J|\sin \phi|, \text{ or } \delta = 0. \quad (\text{B2})$$

For $\phi = 0, \pi$ and $\delta \neq 0$, the monolayer system has time-reversal symmetry (TRS) and the Chern number is zero. When varying ϕ , the Chern number remains zero until the gap closes at $t = J|\sin \phi|$. Thus, the Chern number is nonzero as $t < J|\sin \phi|$. The phase diagram is shown in Fig. 6(a). When $t < J|\sin \phi|$, the gap closing condition $\delta = 0$ separates two nontrivial phases with different Chern numbers as indicated in Fig. 6(b). The energy spectra in Figs. 6(c) and 6(d) are calculated for the open boundary conditions along \mathbf{e}_1 and \mathbf{e}_2 , respectively. They demonstrate the topologically nontrivial phase with chiral edge state.

By our general construction of the bilayer model in the main text, the hopping amplitudes of inserted twisted π -phase blocks are related to the complex hopping amplitude $J e^{i\phi}$ as

$$J_R + iJ_I = J e^{i\phi}. \quad (\text{B3})$$

Then, the Hamiltonian of this bilayer system can be directly obtained from Eqs. (9) and (10) of the main text as

$$\mathcal{H}^{\text{tr}}(\mathbf{k}) = \begin{bmatrix} h_+^{\text{tr}}(\mathbf{k}) & -i h_-^{\text{tr}}(\mathbf{k}) \\ i h_-^{\text{tr}}(\mathbf{k}) & h_+^{\text{tr}}(\mathbf{k}) \end{bmatrix}, \quad (\text{B4})$$

where

$$\begin{aligned} h_+^{\text{tr}}(\mathbf{k}) &= (2J_R \cos \mathbf{k} \cdot \mathbf{e}_1 + 2t \cos \mathbf{k} \cdot \mathbf{e}_2) \sigma_1 \\ &\quad + 2\delta \sin \mathbf{k} \cdot \mathbf{e}_2 \sigma_2 - 2t \cos \mathbf{k} \cdot \mathbf{e}_3 \sigma_3, \\ h_-^{\text{tr}}(\mathbf{k}) &= 2J_I \sin \mathbf{k} \cdot \mathbf{e}_1 \sigma_1. \end{aligned} \quad (\text{B5})$$

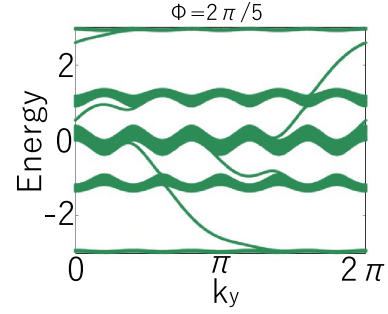


FIG. 7. The spectrum of the monolayer system with $t = J = 1$, and $\phi = 2\pi/5$.

From the relation in Eq. (B3) and the phase diagram of monolayer system in Figs. 6(a) and 6(b), it is now clear that the phases of bilayer system is irrelevant to J_R in Fig. 3(b). When $t < |J_I|$ and $\delta \neq 0$, the mirror Chern number is nonzero, which signifies the existence of mirror Chern insulator.

APPENDIX C: HOFSTADTER MODEL WITH HIGH CHERN NUMBER

The monolayer square lattice of Hofstadter model with gauge flux $\phi = 2\pi/5$ penetrating through each plaquette is illustrated in the upper subfigure of Fig. 4(a). The horizontal hopping amplitude is t , while the vertical one is J . Then, the monolayer Hamiltonian is written as

$$h_C^{\text{Hof}} = \begin{bmatrix} J_0(k_y) & t & 0 & 0 & t e^{-ik_x} \\ t & J_1(k_y) & t & 0 & 0 \\ 0 & t & J_2(k_y) & t & 0 \\ 0 & 0 & t & J_3(k_y) & t \\ t e^{ik_x} & 0 & 0 & t & J_4(k_y) \end{bmatrix}, \quad (\text{C1})$$

where $J_n = 2J \cos(k_y - n\phi)$. The Chern numbers for the five bands are obtained as

$$-1, \quad -1, \quad 4, \quad -1, \quad -1, \quad (\text{C2})$$

written from higher to lower energies, respectively. As shown in Fig. 7, there are four energy gaps with the numbers of chiral edge states as 1, 2, 2, 1 inside them, respectively.

By our construction of bilayer model, the Hamiltonian of bilayer system for mirror Chern insulator can be written as

$$\mathcal{H}^{\text{Hof}}(\mathbf{k}) = \tau_0 \otimes h_+^{\text{Hof}}(\mathbf{k}) + \tau_2 \otimes h_-^{\text{Hof}}(\mathbf{k}) \quad (\text{C3})$$

with

$$h_+^{\text{Hof}}(\mathbf{k}) = \begin{bmatrix} f_0(k_y) & t & 0 & 0 & t e^{-ik_x} \\ t & f_1(k_y) & t & 0 & 0 \\ 0 & t & -f_2(k_y) & t & 0 \\ 0 & 0 & t & -f_3(k_y) & t \\ t e^{ik_x} & 0 & 0 & t & f_4(k_y) \end{bmatrix},$$

and

$$h_-^{\text{Hof}}(\mathbf{k}) = \begin{bmatrix} 0 & 0 & 0 & 0 & 0 \\ 0 & g_1(k_y) & 0 & 0 & 0 \\ 0 & 0 & g_2(k_y) & 0 & 0 \\ 0 & 0 & 0 & -g_3(k_y) & 0 \\ 0 & 0 & 0 & 0 & -g_4(k_y) \end{bmatrix},$$

where $f_0(k_y) = 2J \cos k_y$, $f_n(k_y) = 2J_R^n \cos k_y$, and $g_n(k_y) = 2J_I^n \sin k_y$, for $n = 1, 2, 3, 4$ with (J_R^n, J_I^n) with $n = 1, 2, 3, 4$ given in Fig. 4.

APPENDIX D: THE SIMULATION WITH ACOUSTIC SYSTEM

We review the realization of \mathbb{Z}_2 gauge field in acoustic systems [32,33,35], followed by the proposal for simulating our models as an application. The advantage of using artificial systems rests on the controllable hopping or coupling terms. For example, if there is no coupling between two fixed sites, just remove all the connecting materials between these two sites. For traditional electronic systems, this could be achieved by properly designing the local states with some sorts of symmetries such that the energy integral vanishes. To simulate electronic system by acoustic system, the eigen oscillation mimics the electronic wave function in solid systems. In this way, the equation of motion for electrons is simulated by the dynamic equation of the oscillation in acoustic system with the frequency playing the role of energy. To be precise, lattice sites in solid systems are replaced by acoustic resonators, while hopping between different sites is realized by coupling between different resonators. By connecting the acoustic resonators with wave guides or coupling tubes, the coupling amplitude can be easily controlled since it is completely determined by the radius of wave guide or coupling tube.

To control the sign of the coupling between different resonators, the dipolar mode far away from other modes of the resonator is chosen, which resembles the atomic p orbital as shown in Fig. 8. So, let us begin with the coupling between two remote p_z orbitals in solid system as shown in Figs. 8(a) and 8(b). Assuming the coupling coefficient is t and the on-site energy is ε_0 , the Hamiltonian of this small system can be written as

$$H = \begin{bmatrix} \varepsilon_0 & t \\ t & \varepsilon_0 \end{bmatrix} \quad (\text{D1})$$

with two eigenstates

$$|\pm\rangle = \frac{1}{\sqrt{2}} \begin{bmatrix} 1 \\ \pm 1 \end{bmatrix} \quad (\text{D2})$$

for $E_{\pm} = \varepsilon_0 \pm t$, respectively. If $t < 0$, the low-energy state is bonding state while the high-energy one is antibonding state as shown by Fig. 8(a). The case for $t > 0$ is just opposite as shown in Fig. 8(b). As to the acoustic resonator, the dipolar mode manifests the sinusoidal distribution of air pressure inside the resonator, which just mimics the wave function of p_z orbital. For hopping simulated by coupling different resonators with wave guides, there is a physical picture here. The wave guides introduce the perturbation to eigenmodes of the resonators. In acoustic systems, the uniform distribution of air pressure always has lower frequency or lower energy than the sinusoidal distribution. Therefore, by considering the perturbation from the wave guides in Fig. 8(c), the bonding state has lower frequency than the antibonding one. From the lesson of Fig. 8(a) that the coupling coefficient is negative if the bonding state has lower energy, we obtain the effective coupling $t < 0$. Namely, there is a π hopping phase

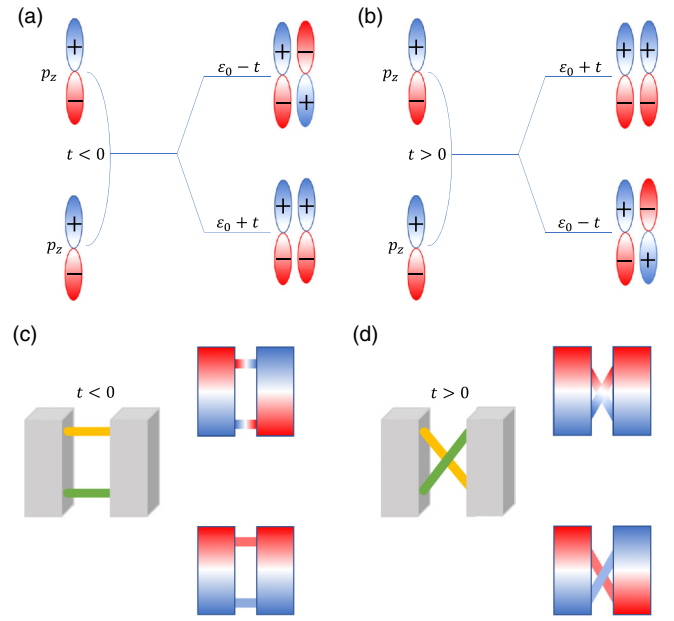


FIG. 8. (a) and (b) illustrate π bonds formed by two p_z orbitals for $t < 0$ and $t > 0$, respectively. For $t < 0$, the bonding state has lower energy, while the antibonding state has higher energy illustrated by the two right configurations of (a). The case for (b) is opposite. (c) and (d) realize the effective coupling $t < 0$ and $t > 0$ in acoustic systems, respectively. The gray cubes denote the acoustic resonators connected by the wave guides (green and yellow sticks), and the positive and negative air pressures are marked with blue and red colors.

for the connection structure of Fig. 8(c). The case of Fig. 8(d) is just opposite to that of Fig. 8(c). In this way, the \mathbb{Z}_2 gauge field can be readily realized in acoustic systems by properly designing the connection structures.

The above strategy of controlling the coupling between acoustic resonators, as a proven technology, has been widely used in topological acoustic systems. We now turn to the realization of our models. It is clear that once the building blocks in Fig. 2 are simulated, our models are immediately realized. We illustrate the realization of the building blocks in Fig. 2(b) by Fig. 9, and the realization of building blocks of Fig. 2(c) is just similar. In Fig. 9, the red and blue

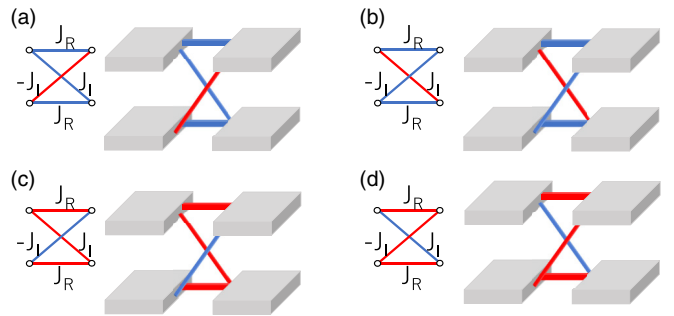


FIG. 9. Realization of building blocks in Fig. 2(b) of the main text. The red and blue links connecting different acoustic resonators represent the connection structures in Figs. 8(c) and 8(d), respectively.

connections between different acoustic resonators represent the connection structures of Figs. 8(c) and 8(d), respectively. As to the realistic experimental setup, the mature 3D-printing

technique with photosensitive resin has been demonstrated to be a powerful method of realizing all these models in acoustic systems.

-
- [1] K. v. Klitzing, G. Dorda, and M. Pepper, New method for high-accuracy determination of the fine-structure constant based on quantized Hall resistance, *Phys. Rev. Lett.* **45**, 494 (1980).
- [2] D. J. Thouless, M. Kohmoto, M. P. Nightingale, and M. den Nijs, Quantized Hall conductance in a two-dimensional periodic potential, *Phys. Rev. Lett.* **49**, 405 (1982).
- [3] F. D. M. Haldane, Model for a quantum Hall effect without Landau levels: Condensed-matter realization of the “parity anomaly”, *Phys. Rev. Lett.* **61**, 2015 (1988).
- [4] G. Jotzu, M. Messer, R. Desbuquois, M. Lebrat, T. Uehlinger, D. Greif, and T. Esslinger, Experimental realization of the topological Haldane model with ultracold fermions, *Nature (London)* **515**, 237 (2014).
- [5] C. L. Kane and E. J. Mele, Z_2 topological order and the quantum spin Hall effect, *Phys. Rev. Lett.* **95**, 146802 (2005).
- [6] C. L. Kane and E. J. Mele, Quantum spin Hall effect in graphene, *Phys. Rev. Lett.* **95**, 226801 (2005).
- [7] J. C. Y. Teo, L. Fu, and C. L. Kane, Surface states and topological invariants in three-dimensional topological insulators: Application to $\text{Bi}_{1-x}\text{Sb}_x$, *Phys. Rev. B* **78**, 045426 (2008).
- [8] T. H. Hsieh, H. Lin, J. Liu, W. Duan, A. Bansil, and L. Fu, Topological crystalline insulators in the SnTe material class, *Nat. Commun.* **3**, 982 (2012).
- [9] Y. Tanaka, Z. Ren, T. Sato, K. Nakayama, S. Souma, T. Takahashi, K. Segawa, and Y. Ando, Experimental realization of a topological crystalline insulator in SnTe, *Nat. Phys.* **8**, 800 (2012).
- [10] M. Z. Hasan and C. L. Kane, Colloquium: Topological insulators, *Rev. Mod. Phys.* **82**, 3045 (2010).
- [11] X.-L. Qi and S.-C. Zhang, Topological insulators and superconductors, *Rev. Mod. Phys.* **83**, 1057 (2011).
- [12] A. Bansil, H. Lin, and T. Das, Colloquium: Topological band theory, *Rev. Mod. Phys.* **88**, 021004 (2016).
- [13] C.-K. Chiu, J. C. Y. Teo, A. P. Schnyder, and S. Ryu, Classification of topological quantum matter with symmetries, *Rev. Mod. Phys.* **88**, 035005 (2016).
- [14] L. Fu, Topological crystalline insulators, *Phys. Rev. Lett.* **106**, 106802 (2011).
- [15] T. Zhang, Y. Jiang, Z. Song, H. Huang, Y. He, Z. Fang, H. Weng, and C. Fang, Catalogue of topological electronic materials, *Nature (London)* **566**, 475 (2019).
- [16] M. G. Vergniory, L. Elcoro, C. Felser, N. Regnault, B. A. Bernevig, and Z. Wang, A complete catalogue of high-quality topological materials, *Nature (London)* **566**, 480 (2019).
- [17] F. Tang, H. C. Po, A. Vishwanath, and X. Wan, Comprehensive search for topological materials using symmetry indicators, *Nature (London)* **566**, 486 (2019).
- [18] A. Alexandradinata, C. Fang, M. J. Gilbert, and B. A. Bernevig, Spin-orbit-free topological insulators without time-reversal symmetry, *Phys. Rev. Lett.* **113**, 116403 (2014).
- [19] Y. Ando and L. Fu, Topological crystalline insulators and topological superconductors: From concepts to materials, *Annu. Rev. Condens. Matter Phys.* **6**, 361 (2015).
- [20] Z. Yang, F. Gao, X. Shi, X. Lin, Z. Gao, Y. Chong, and B. Zhang, Topological acoustics, *Phys. Rev. Lett.* **114**, 114301 (2015).
- [21] F. Li, X. Huang, J. Lu, J. Ma, and Z. Liu, Weyl points and Fermi arcs in a chiral phononic crystal, *Nat. Phys.* **14**, 30 (2018).
- [22] G. Ma, M. Xiao, and C. T. Chan, Topological phases in acoustic and mechanical systems, *Nat. Rev. Phys.* **1**, 281 (2019).
- [23] L. Lu, J. D. Joannopoulos, and M. Soljačić, Topological photonics, *Nat. Photonics* **8**, 821 (2014).
- [24] Y. Yang, Z. Gao, H. Xue, L. Zhang, M. He, Z. Yang, R. Singh, Y. Chong, B. Zhang, and H. Chen, Realization of a three-dimensional photonic topological insulator, *Nature (London)* **565**, 622 (2019).
- [25] T. Ozawa, H. M. Price, A. Amo, N. Goldman, M. Hafezi, L. Lu, M. C. Rechtsman, D. Schuster, J. Simon, O. Zilberberg, and I. Carusotto, Topological photonics, *Rev. Mod. Phys.* **91**, 015006 (2019).
- [26] S. Imhof, C. Berger, F. Bayer, J. Brehm, L. W. Molenkamp, T. Kiessling, F. Schindler, C. H. Lee, M. Greiter, T. Neupert, and R. Thomale, Topoelectrical-circuit realization of topological corner modes, *Nat. Phys.* **14**, 925 (2018).
- [27] R. Yu, Y. X. Zhao, and A. P. Schnyder, 4D spinless topological insulator in a periodic electric circuit, *Natl. Sci. Rev.* **7**, 1288 (2020).
- [28] E. Prodan and C. Prodan, Topological phonon modes and their role in dynamic instability of microtubules, *Phys. Rev. Lett.* **103**, 248101 (2009).
- [29] R. Süssstrunk and S. D. Huber, Observation of phononic helical edge states in a mechanical topological insulator, *Science* **349**, 47 (2015).
- [30] S. D. Huber, Topological mechanics, *Nat. Phys.* **12**, 621 (2016).
- [31] J. Dalibard, F. Gerbier, G. Juzeliūnas, and P. Öhberg, Colloquium: Artificial gauge potentials for neutral atoms, *Rev. Mod. Phys.* **83**, 1523 (2011).
- [32] H. Xue, Y. Ge, H.-X. Sun, Q. Wang, D. Jia, Y.-J. Guan, S.-Q. Yuan, Y. Chong, and B. Zhang, Observation of an acoustic octupole topological insulator, *Nat. Commun.* **11**, 2442 (2020).
- [33] Y. Qi, C. Qiu, M. Xiao, H. He, M. Ke, and Z. Liu, Acoustic realization of quadrupole topological insulators, *Phys. Rev. Lett.* **124**, 206601 (2020).
- [34] X. Ni, M. Li, M. Weiner, A. Alù, and A. B. Khanikaev, Demonstration of a quantized acoustic octupole topological insulator, *Nat. Commun.* **11**, 2108 (2020).
- [35] H. Xue, Z. Wang, Y.-X. Huang, Z. Cheng, L. Yu, Y. X. Foo, Y. X. Zhao, S. A. Yang, and B. Zhang, Projectively enriched symmetry and topology in acoustic crystals, *Phys. Rev. Lett.* **128**, 116802 (2022).
- [36] T. Li, J. Du, Q. Zhang, Y. Li, X. Fan, F. Zhang, and C. Y. Qiu, Acoustic Möbius insulators from projective symmetry, *Phys. Rev. Lett.* **128**, 116803 (2022).
- [37] X.-G. Wen, Quantum orders and symmetric spin liquids, *Phys. Rev. B* **65**, 165113 (2002).

- [38] Y. X. Zhao, Y.-X. Huang, and S. A. Yang, z_2 -projective translational symmetry protected topological phases, *Phys. Rev. B* **102**, 161117(R) (2020).
- [39] Y. X. Zhao, C. Chen, X.-L. Sheng, and S. A. Yang, Switching spinless and spinful topological phases with projective PT symmetry, *Phys. Rev. Lett.* **126**, 196402 (2021).
- [40] L. B. Shao, Q. Liu, R. Xiao, S. A. Yang, and Y. X. Zhao, Gauge-field extended $k \cdot p$ method and novel topological phases, *Phys. Rev. Lett.* **127**, 076401 (2021).
- [41] Z. Y. Chen, S. A. Yang, and Y. X. Zhao, Brillouin Klein bottle from artificial gauge fields, *Nat. Commun.* **13**, 2215 (2022).
- [42] Y.-X. Huang, Z. Y. Chen, X. Feng, S. A. Yang, and Y. X. Zhao, Periodic clifford symmetry algebras on flux lattices, *Phys. Rev. B* **106**, 125102 (2022).
- [43] Z. Y. Chen, Z. Zhang, S. A. Yang, and Y. X. Zhao, Classification of time-reversal-invariant crystals with gauge structures, *Nat. Commun.* **14**, 743 (2023).
- [44] C. Zhang, Z. Y. Chen, Z. Zhang, and Y. X. Zhao, General theory of momentum-space nonsymmorphic symmetry, *Phys. Rev. Lett.* **130**, 256601 (2023).
- [45] Y. Deng and Y. Jing, Acoustic crystals with a Möbius twist, *Physics* **15**, 36 (2022).
- [46] H. Xue, Z. Y. Chen, Z. Cheng, J. X. Dai, Y. Long, Y. X. Zhao, and B. Zhang, Stiefel-Whitney topological charges in a three-dimensional acoustic nodal-line crystal, *Nat. Commun.* **14**, 4563 (2023).
- [47] One may redefine the mirror operator as $\tilde{\mathcal{M}} = -i\mathcal{M}$. Since \mathcal{T} is anti-unitary, the algebra in (1) would be translated to an equivalent form of $\{\mathcal{T}, \tilde{\mathcal{M}}\} = 0$ and $\tilde{\mathcal{M}}^2 = 1$. In the following discussion, we shall stick to the form in (1).
- [48] S.-Q. Shen, *Topological Insulators* (Springer, New York, 2012).
- [49] B. Bernevig and T. Hughes, *Topological Insulators and Topological Superconductors* (Princeton University Press, Princeton, NJ, 2013).
- [50] D. R. Hofstadter, Energy levels and wave functions of Bloch electrons in rational and irrational magnetic fields, *Phys. Rev. B* **14**, 2239 (1976).
- [51] M. Kohmoto, Topological invariant and the quantization of the Hall conductance, *Ann. Phys.* **160**, 343 (1985).
- [52] The parameters are not required to be accurate. The topological phase is robust under the deformation of parameters as long as the mirror symmetry is preserved and the energy gap is not closed.
- [53] D.-W. Zhang, Y.-Q. Zhu, Y. X. Zhao, H. Yan, and S.-L. Zhu, Topological quantum matter with cold atoms, *Adv. Phys.* **67**, 253 (2018).
- [54] N. R. Cooper, J. Dalibard, and I. B. Spielman, Topological bands for ultracold atoms, *Rev. Mod. Phys.* **91**, 015005 (2019).